The Frequency Behavior of the Third-Order Intercept Point in a Waveguide Photodiode

H. Jiang, D. S. Shin, G. L. Li, T. A. Vang, D. C. Scott, and P. K. L. Yu

***Abstract*—In Hayes's (1993) and Williams's (1996) analyses, the photodiode nonlinearity is attributed to the space charge screening effect. In this paper, the third-order intermodulation distortions of a high frequency, large optical cavity p-i-n waveguide photodiode are characterized up to 18 GHz using a two-tone measurement. At high bias voltage, the third-order intercept point (IP3) of the waveguide photodiode is constant at low frequency and $\sim f^{-3}$ at high frequency. This closely agrees with our model, which is based upon variation of the photodiode impedance. The measured IP3 of the same device at low bias voltages indicates the contribution of space charge screening under low bias voltage or severe saturation.**

***Index Terms*—Analog fiber-optic link, intermodulation distortion, large optical cavity waveguide, photodiode.**

IN analog fiber-optic links, the linearity of the photodiode is critical in the dynamic range consideration of the link. For single-octave applications, the two-tone third-order intermodulation distortions (IMD3) attract particular attention as their frequencies are close to the fundamental signals. While a high IP3 is essential for large spurious-free dynamic range (SFDR), the frequency dependence of IP3 is an important feature in the design of frequency agile links.

Presently, there are two models that describe the frequency behavior of photodiode harmonic distortions. In [1], [2], harmonic distortions of the p-i-n photodiode were modeled with nonuniform transit velocity of carriers in the low electric field region caused by the photogenerated space charge screening. In [3], we showed that the harmonic distortion levels of unsaturated p-i-n waveguide photodiode could be related to the variation of the microwave impedance of the photodiode under illumination with the diode treated as a part of the closed loop detection circuit. In this model, nonlinear distortions were calculated using an equivalent circuit with the impedance extracted from the photodiode's microwave reflection coefficient (S_{11}). The junction capacitance variation was used to estimate the harmonic distortions before severe saturation occurs.

In principle, the intermodulation distortions can be estimated from the harmonic distortions in both models. However, due to the intrinsic frequency dependence of the photodiode, it can be inaccurate, especially at high frequency, to infer the two-tone intermodulation distortions from the one-tone harmonic distortions. In this work, a two-tone setup employing two lasers and two modulators is used to characterize the IMD3 of a high performance, large optical cavity InGaAs–InP waveguide photodiode. Our setup is an extension of the Ozeki's direct modulation scheme [4]. At high bias, we extend the S_{11} analysis in [3] and compare the IP3's predicted from the nonlinear impedance model with those measured directly. Our measurement results confirm the conditions for the nonlinear impedance model and the nonuniform transit velocity model to be applicable.

The large optical cavity waveguide p-i-n photodiode used in this experiment consists of an undoped, 0.12-μm-thick InGaAs absorption layer sandwiched between two 1.2-μm-thick InGaAsP ($\lambda_g = 1.15\,\mu$m) layers, followed by 0.4-μm-thick InP cladding layers. The topmost layer is a 0.05-μm-thick p^+-InGaAs. After epitaxy, a 4-μm-wide waveguide is etched via wet chemical etching. A goldplated air bridge is used to connect the top of the mesa to a coplanar waveguide transmission line on the semi-insulating InP substrate [6]. For AR-coated devices, the coupling efficiency of the waveguide to a tapered fiber with a 3.5-μm spot size is estimated [using the beam propagation method (BPM)] at 90% and is polarization insensitive, while the optical confinement factor (Γ) of the absorption layer is 10%. The small Γ is for reducing the optical saturation at the front end of the photodiode. A portion $\sim 0.15\ \mu$m of the InGaAsP layers next to the absorption layer is undoped, and the total intrinsic region thickness is 0.45 μm. For the uncoated device that has a 55-μm long waveguide, we measure a 3-dBe bandwidth of 35 GHz and a small signal RF responsivity of 0.53 A/W (using HP8703 optical network analyzer) at 20 GHz (and 0.62 A/W at DC).

To characterize the responsivity at different illuminations, the microwave output power of the photodiode is measured as the average incident optical power is varied. A 100% modulated optical signal is generated by the optical heterodyne method using two temperature-tuned, 1.32-μm wavelength Nd:YAG lasers with similar optical power and polarization. The microwave power detected by the photodiode increases linearly in the log–log scale (with a slope of 2) with the total optical power, until compression occurs. At 20 GHz, the microwave 1-dB compression point of this device is measured at 6.2 mA of dc photocurrent and at -4 dBm of microwave output power that includes the microwave loss of the cable and the probe.

For the IP3 measurement, we use the two-tone setup depicted in Fig. 1, where each optical link consists of a Nd:YAG laser and a Mach–Zehnder modulator (MZM). The MZM's are modulated at f_1 and f_2, respectively. The 3-dB optical coupler combines the two modulated optical signals. The polarization-independent optical attenuator changes the optical power coupled to

Manuscript received October 11, 1999; revised January 17, 2000. This work was supported by TRW. This work was presented in part at the IEEE Microwave Photonics Conference, Melbourne, Australia, November 1999.

H. Jiang is with Conexant Inc., Newport Beach, CA 92660 USA.

D. S. Shin, G. L. Li, and P. K. L. Yu are with the Department of Electrical and Computer Engineering, University of California at San Diego, La Jolla, CA 92093-0407 USA.

T. A. Vang and D. C. Scott are with TRW, Redondo Beach, CA 90278 USA.

Publisher Item Identifier S 1041-1135(00)03614-4.

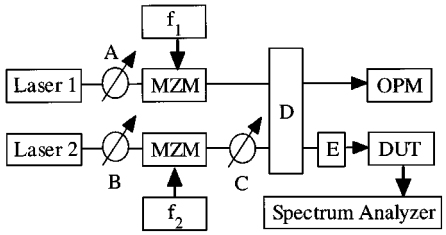

Fig. 1. Two-tone setup for measuring the IP3 of the photodiode. A, B, and C are polarization rotators, D is a 3-dB coupler, E is an optical attenuator, OPM stands for optical power meter, and DUT for device under test. The microwave sources contain an isolator and a bandpass filter.

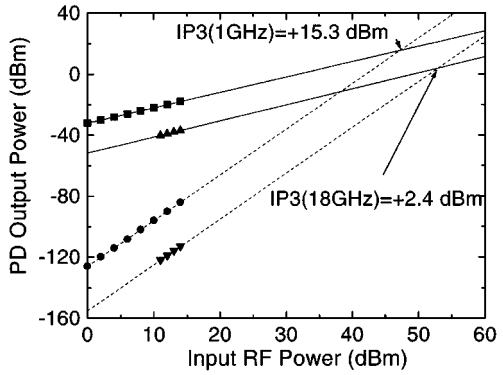

Fig. 2. Measured fundamental (■) and IMD3 (•) signals at 1 GHz, and measured fundamental (▲) and IMD3 (▼) at 18 GHz versus input RF power, at 2.2 mA photocurrent and -9 V bias.

the photodiode. Polarization rotators A and B are used before the modulators to maximize the modulation efficiency. This is similar in concept to the setup in [4]. In our approach, by biasing the MZM at the quadrature point to minimize the second-harmonic distortions (HD2), the second-order intermodulation distortions at $2f_1 - f_2$ and $2f_2 - f_1$, arising from the second harmonic of one tone and the fundamental of the other tone, can be minimized. Therefore, the IMD3 at the photodiode can be more accurately measured. This, together with appropriate microwave isolators and bandpass filters between the microwave synthesizers and the modulators, results in a larger than 50 dBc suppression of the HD2. The extra spurious signals due to the beating of the two free running Nd:YAG lasers can be minimized by rotating the polarization rotator C so that the beams become orthogonally polarized. A spectrum analyzer is used to measure the fundamental and the IMD3 signals at the photodiode output at different input microwave powers. Fig. 2 shows two sets of measurement results with f_1 and f_2 set at 1 and 1.04 GHz, and 18.00 and 18.04 GHz, respectively, at -9 V bias. The output-referenced IP3 is extrapolated from the fundamental and the IMD3.

The S_{11} of the photodiode at different optical power levels is measured from 200 MHz to 20 GHz at the source power setting of -10 dBm [6]. The equivalent circuit model for the p-i-n photodiode is shown in Fig. 3 [3]. The junction capacitance C_j and resistance R_j of the waveguide photodiode at different photocurrents are extracted from the S_{11} data and are listed in Table I for $-3, -6$ and -9 V biases, respectively. The series resistance R_s and the parasitic capacitance C_p are found to be 22 Ω and 0.035 pF, respectively, for all photocurrent and bias levels.

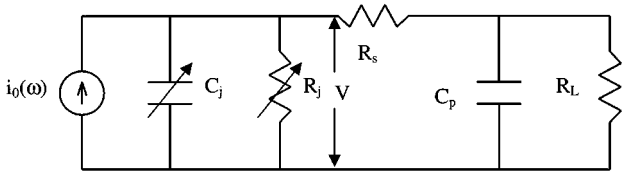

Fig. 3. Equivalent circuit model for the p-i-n photodiode under illumination.

TABLE I
JUNCTION CAPACITANCE (IN fF) AND RESISTANCE (IN kΩ) OF THE PHOTODIODE UNDER DIFFERENT BIASES AND PHOTOCURRENTS (IN mA)

i	-9V		-6V		3V	
	R_j	C_j	R_j	C_j	R_j	C_j
0	1000	40.1	1000	40.1	67.9	40.1
1	44.9	41.0	41.8	41.0	36.5	41.1
2	30.3	41.7	24.8	41.7	10.9	41.8
3	13.4	42.6	8.49	42.7	1.02	42.9
4	11.7	43.1	7.69	43.2	0.97	43.4

We have extended the equivalent circuit model of p-i-n photodiode in [4] to calculate the IP3 using the extracted impedances. The voltage V across the current source (from which we obtain the voltage across the load) is calculated from [7]

$$\frac{d}{dt}\{(C_0 + iC_1)V\} + \frac{V}{R_0 - iR_1} + \frac{V}{Z(\omega)} = i \qquad (1)$$

where $i = i_0(\cos(\omega_1 t) + \cos(\omega_2 t))$ represents the two RF current sources, $Z(\omega)$ is the equivalent impedance of C_p, R_s, and the load resistance R_L. For simplicity, we take the small signal, linear approximation, where C_j is taken to increase linearly with the input optical power, and C_1 is the optical power-dependent differential capacitance. Likewise, R_j decreases linearly with the optical power and R_1 is the optical power-dependent differential resistance. The increase of junction capacitance can be explained by an increase in the electric polarization due to the photogenerated electron hole pairs, whose density depends on the net electric field and optical illumination [8]. C_0 and R_0 are the respective capacitance and resistance of the junction at a given dc photocurrent. If $R_0 \gg iR_1$, the junction conductance can be approximated as

$$\frac{1}{R_0 - iR_1} = \frac{1}{R_0}\left[1 + i\frac{R_1}{R_0} + \left(i\frac{R_1}{R_0}\right)^2 + \cdots\right]. \qquad (2)$$

Using the Harmonic Balance Method (HBM), V can be expanded as

$$\begin{aligned} V = {} & (V_{a1}\cos(\omega_1 t) + V_{b1}\sin(\omega_1 t)) \\ & + (V_{a2}\cos(\omega_2 t) + V_{b2}\sin(\omega_2 t)) \\ & + (V_{a3}\cos(2\omega_1 t) + V_{b3}\sin(2\omega_1 t)) \\ & + (V_{a4}\cos(2\omega_2 t) + V_{b4}\sin(2\omega_2 t)) \\ & + (V_{a5}\cos((\omega_1 - \omega_2)t) + V_{b5}\sin((\omega_1 - \omega_2)t)) \\ & + (V_{a6}\cos((\omega_1 + \omega_2)t) + V_{b6}\sin((\omega_1 + \omega_2)t)) \\ & + (V_{a7}\cos((2\omega_1 - \omega_2)t) + V_{b7}\sin((2\omega_1 - \omega_2)t)) + \cdots \end{aligned} \qquad (3)$$

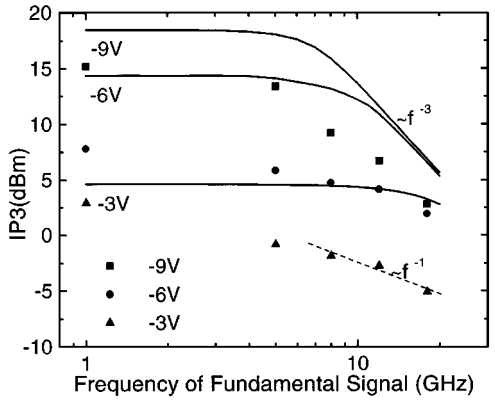

Fig. 4. IP3 of the waveguide photodiode at different biases as a function of frequency. Solid curves represent prediction from nonlinear impedance and S_{11} analysis, and ■, ●, and ▲ are from direct measurement at 2.2 mA photocurrent.

Inserting (3) into (1) and using the orthogonality property of sine and cosine functions, we obtain a set of linear equations for V_{ai} and V_{bi}. In this way, fundamental signal at f_1 and IMD3 at $2f_1 - f_2$ can be expressed as a function of the circuit parameters, from which IP3 can be obtained. The equivalent circuit parameters of the photodiode are extracted from S_{11} measurements at each optical level.

The solid curves in Fig. 4 depict the IP3 frequency behavior predicted from the nonlinear impedance model at 2 mA of photocurrent. The variation of IP3 can be qualitatively understood as follows. In the measured frequency range, both the variations of the junction capacitance and resistance contribute to the IMD3 via the overall junction impedance variation. The portion of the IMD3 caused by the R_j variation is frequency independent, and this portion dominates at low frequency. As frequency increases, the IMD3 generated by the C_j variation gradually prevails because the admittance of the capacitor goes like $j\omega C$. In the above analysis, we found that V_{a7} and V_{b7} are dominated by ΔC_j contribution and both go like $(2f_1 - f_2)^3$. Therefore, IP3 $\sim (2f_1 - f_2)^{-3}$ at high frequency. As mentioned, IP3 also has contribution from the nonuniform transit velocity effect due to photogenerated carriers [1], [2]. Hayes *et al.* concluded that the amplitude of IMD3 is proportional to the $(2f_1 - f_2)$ at a certain fixed bias and dc photocurrent [1]. Therefore, IP3 would go like $\sim(2f_1 - f_2)^{-1}$ at higher frequency when the nonuniform transit velocity effect is dominant.

With the two-tone setup in Fig. 1, the IP3's of the same device are measured at -3 V, -6 V, and -9 V bias and at a photocurrent of 2.2 mA. They are also plotted (as ■, ●, and ▲) in Fig. 4. The low bias case corresponds to the situation of severe saturation, even at moderate optical power. f_1 is set at 1, 8, 12, and 18 GHz, respectively, while f_2 is set at $f_1 + 40$ MHz. At -9-V bias, the measured IP3's are within a few dB of the solid curve and are within the accuracy of C_1 and R_1. The same IP3 frequency behavior, as discussed above, is observed in the two-tone measurement, suggesting the dominance of nonlinear impedance effect at this bias. At -3 V, the frequency dependence of IP3 deviates from the solid curve. From 8 to 18 GHz, the measured IP3 $\sim f^{-}1$. The IMD3 caused by nonuniform velocity effect dominates here because the applied electric field $\sim$67 kV/cm approaches the threshold electric field $\sim$50 kV/cm for space charge pile-up [2]. At -6 V, both effects contribute to the nonlinear distortion in the photodiode.

From the measured IP3, the SFDR of the shot-noise limited fiber optic link (detector limited) with the photodiode biased at -9 V is estimated at 120 dB/Hz$^{2/3}$ at 1 GHz, and 112 dB/Hz$^{2/3}$ at 18 GHz, at 2.2 mA photocurrent. This photodiode can be useful in analog links with linearized modulator [9] or at high photocurrent [10].

In summary, we have demonstrated that at high voltage, the nonlinear impedance model provides a good fitting to the IP3 of the waveguide photodiode and explains its frequency dependence. The IP3 measurement of the photodiode at low bias voltage is consistent with that expected of the nonuniform transit velocity effect at low electric field or under severe optical saturation. In this work, we have also characterized a large optical cavity waveguide p-i-n photodiode that has a 3-dBe bandwidth of 35 GHz, a small signal RF-responsivity of 0.53 A/W at 20 GHz, and a 1-dB compression point of 6.2 mA (with 100% modulation) at 20 GHz.

ACKNOWLEDGMENT

The authors would like to specially thank Dr. S. A. Pappert for the loan of the Nd:YAG lasers and modulators for this work.

REFERENCES

[1] R. R. Hayes and D. L. Persechini, "Nonlinearity of p-i-n photodetectors," *IEEE Photon. Technol. Lett.*, vol. 5, pp. 70–72, Mar. 1993.

[2] K. J. Williams, R. D. Esman, and M. Dagenais, "Nonlinearities in p-i-n microwave photodetectors," *J. Lightwave Technol.*, vol. 14, pp. 84–96, 1996.

[3] H. Jiang and P. K. L. Yu, "Equivalent circuit analysis of harmonic distortions in photodiode," *IEEE Photon. Technol. Lett.*, vol. 10, pp. 1608–1610, Nov. 1998.

[4] T. Ozeki and E. H. Hara, "Measurement of nonlinear distortion in photodiodes," *IEEE Electron. Lett.*, vol. 12, no. 3, pp. 80–81, 1976.

[5] H. Jiang, J. T. Zhu, A. L. Kellner, and P. K. L. Yu, "A high power asymmetric waveguide InGaAs photodetector operating at 76 mW optical power," in *Proc. SPIE*, vol. 2844, 1996, pp. 120–124.

[6] P. Debie, L. Martens, and D. Kaiser, "Improved error correction technique for on-wafer lightwave measurement of photodetectors," *IEEE Photon. Technol. Lett.*, vol. 7, pp. 418–420, June 1995.

[7] H. Jiang, D. S. Shin, G. L. Li, J. T. Zhu, T. A. Vang, and P. K. L. Yu, "Analysis of IP3 of photodiode using equivalent circuit," in *IEEE Microwave Photonics Conf., MWP'99*, Paper T-5.3, Melbourne, Australia, Nov. 1999.

[8] J. E. Villet, S. Mottet, L. L. Juerou, and C. Boisrobert, "Photodiode for coherent detection: Modeling and experimental results," *J. Phys. C4*, vol. 49, pp. 321–324, Sept. 1988.

[9] J. A. Schaffner and W. B. Bridges, "Intermodulation distortion in high dynamic range microwave fiber-optic links with linearized modulators," *J. Lightwave Technol. Lett.*, vol. 11, pp. 3–6, 1993.

[10] K. J. Williams, L. T. Nichols, and R. D. Esman, "Photodetector nonlinearity limitations on a high-dynamic range 3 GHz fiber optic link," *J. Lightwave Technol. Lett.*, vol. 16, pp. 192–199, 1998.